AIChE Annual Meeting, Salt Lake City, USA, Nov. 4-9, 2007

PURELY-ELASTIC FLOW INSTABILITIES IN A MICROFLUIDIC CROSS-SLOT GEOMETRY

Robert J. Poole, Dep. of Engineering, University of Liverpool, United Kingdom
Manuel A. Alves, CEFT, Departamento de Engenharia Química, FEUP, Porto, Portugal
Alexandre P. Afonso, CEFT, Departamento de Engenharia Química, FEUP, Porto, Portugal
Fernando T. Pinho, CEFT, FEUP, Porto, Portugal and Universidade do Minho, Braga, Portugal
Paulo J. Oliveira, UMTP, Departamento de Engenharia Electromecânica, UBI, Covilhã, Portugal

Abstract

In this work we demonstrate numerically, using a 3D finite-volume method, that viscoelastic flow in a microfluidic cross-slot geometry can lead to flow asymmetries under perfectly symmetric flow conditions. This supercritical instability is predicted using the upper-convected Maxwell model under creeping flow conditions, thus demonstrating that it is purely elastic in nature. The numerical results obtained agree qualitatively with the recent experimental findings of Arratia et al. [1].

We investigate the effect of the aspect ratio of the geometry, showing the stabilizing effect of the upper and lower walls. In the limit of small depth a Hele-Shaw flow is approached and the onset of asymmetric flow is suppressed. On the other hand, the elastic instability that leads to a periodic flow occurs at increasingly smaller Deborah numbers as the aspect ratio decreases.

Introduction

The flow of viscoelastic fluids often leads to counter-intuitive flow features as illustrated in the compilation of flow-visualization photographs presented in the book by Boger and Walters [2]. It is now well establish that viscoelastic flows often produce purely-elastic flow instabilities [3-8], which lead to unsteady flows, even under inertia-less flow conditions (i.e. $Re \rightarrow 0$). A promising use of this nonlinear behavior of complex fluids is to enhance the mixing of two fluids under low Reynolds number flow conditions [9,10]. As is well known, for Newtonian flows the absence of inertia leads to difficulties in the mixing processes, as described in Ottino and Wiggins [11], for example. On the other hand, as the dimensions of the flow geometry decrease the Reynolds number will also decrease, leading to the characteristic mixing difficulties observed when using Newtonian fluids in microfluidic chips. For viscoelastic fluids, the reduction in the geometry size naturally leads to a considerable increase of the Deborah number, defined as the ratio between the relaxation time of the fluid and the characteristic time of the flow, even when dealing with fluids with relaxation times of the order of milliseconds, which at *macro* flow scales would behave almost as Newtonian liquids [12,13].

Recently, Arratia et al. [1] described a new type of flow instability associated with viscoelasticity, for the flow in a microscale "cross-slot" geometry. It was observed that, even in a symmetric geometry under perfectly symmetric flow conditions, above a critical flow rate (or Deborah number) the flow patterns evolved progressively to develop a steady flow asymmetry. Poole et al. [14] simulated the two-dimensional cross-slot flow of an Upper-Convected Maxwell (UCM) viscoelastic fluid, using a finite-volume methodology [15], and were able to capture qualitatively this supercritical

bifurcation, under creeping-flow conditions. Increasing further the Deborah number produced a second instability where the flow became time-dependent. In the numerical work of Poole et al. [14] it was also shown that increasing the degree of flow inertia (i.e. increasing Reynolds number) leads to a shift of the critical Deborah number to higher values, and a considerable decrease of the flow asymmetry.

In the present work we extend the study of Poole et al. [14] by considering the effect of the three-dimensional nature of the real microfluidic cross slot flow (as in [1]) and investigate in detail the effect of the aspect ratio of the geometry, by varying the depth of the cross slot from low values (quasi-Hele Shaw flow) up to very large values (quasi-two dimensional flow).

Numerical Method and Computational Meshes

The cross-slot geometry is illustrated in Figure 1, where a description of relevant variables is also provided. The inlet and outlet "arms" are ten channel widths (D) in length and fully-developed velocity (with an average value U) and stress profiles at inlets and Neumann boundary conditions at the outlets are imposed. We have confirmed that increasing further the inlet and outlet arm lengths had a negligible effect on the critical De and on the flow patterns. The aspect ratio of the cross slot, here defined as $AR = H / D$, where H represents the depth of the geometry, was varied from 0.01 up to 100. The limiting case of a two-dimensional flow ($AR \to \infty$) was already investigated in a previous work [14], essentially by considering only one cell in the z direction, and imposing symmetry flow boundary conditions on the top and bottom faces ($z / H = \pm 1/2$).

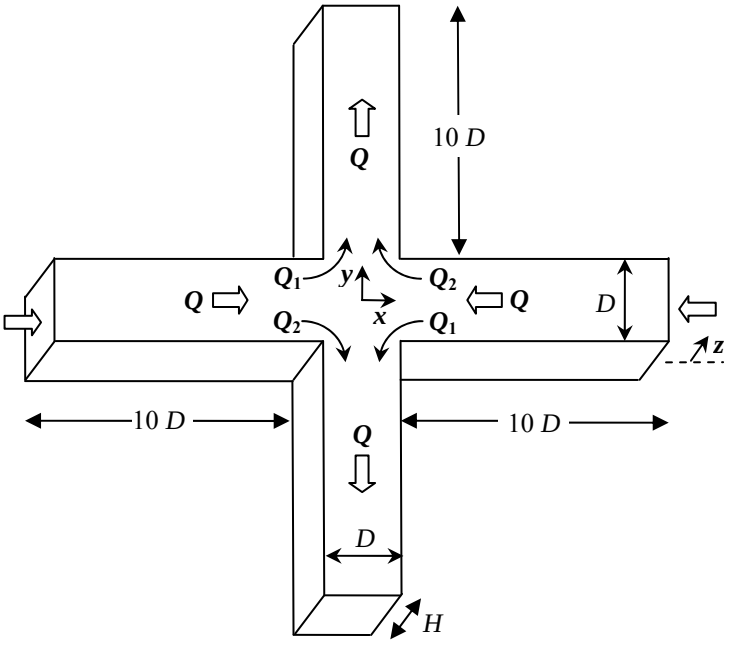

Figure 1. Schematic of the cross slot geometry.

The equations we need to solve are those of conservation of mass

$$\nabla \cdot \mathbf{u} = 0 \tag{1}$$

and linear momentum

$$\rho \frac{\partial \mathbf{u}}{\partial t} + \rho \nabla \cdot \mathbf{u}\mathbf{u} = -\nabla p + \nabla \cdot \boldsymbol{\tau} \tag{2}$$

together with an appropriate constitutive equation for the extra stress $\boldsymbol{\tau}$. Here, as in our previous work [14], we use the UCM model to specify $\boldsymbol{\tau}$,

$$\boldsymbol{\tau} + \lambda \left(\frac{\partial \boldsymbol{\tau}}{\partial t} + \nabla \cdot \mathbf{u}\boldsymbol{\tau} \right) = \eta \left(\nabla \mathbf{u} + \nabla \mathbf{u}^{\mathrm{T}} \right) + \lambda \left(\boldsymbol{\tau} \cdot \nabla \mathbf{u} + \nabla \mathbf{u}^{\mathrm{T}} \cdot \boldsymbol{\tau} \right) \tag{3}$$

where λ and η are the relaxation time and shear viscosity of the fluid, respectively. In this work we will focus on creeping-flow conditions, and as such the advective term in the momentum equation is not included. We will analyze the effect of the aspect ratio, *AR*, and of the Deborah number ($De \equiv \lambda U/D$) on the flow patterns. A finite-volume technique is used to solve Equations (1)-(3). The numerical technique has been described in detail elsewhere [15-18] and therefore is not unnecessarily repeated here.

The mesh used in the numerical simulations is composed of 78 125 cells. A zoomed view near the center of the cross slot is shown in Figure 2. The number of cells in the central cuboidic region of the cross slot is 25 along each direction (x, y and z), leading to minimum cell sizes of $\Delta x/D = \Delta y/D = \Delta z/D = 0.04$. Due to the three-dimensional nature of the flow, further refinement of the mesh leads to significant increases in the required CPU times, and therefore in this preliminary study we decided not to further refine the mesh. In order to assess the adequacy of this level of refinement we present in Figure 3 a comparison of the results obtained, for the limiting two-dimensional case, using 25 cells in the center of the cross slot, with those obtained by Poole et al. [14] using 101 cells in both the x and y directions. To quantify the flow asymmetry, we find useful to define the following parameter [14]

$$DQ = (Q_2 - Q_1)/(Q_1 + Q_2) \tag{4}$$

where Q_1 and Q_2 correspond to the partial flow rates that split into each outlet arm of the cross slot, as illustrated in Figure 1. The total flow rate fed to each inlet channel $Q = Q_1 + Q_2$ splits into either the upper outflow arm (Q_2 in case of "right" arm) or the lower outflow arm (Q_1 in the case of the "right" arm) as shown in Figure 1. We note that $DQ = 0$ for a symmetric flow, while for a completely asymmetric flow *DQ* asymptotes to ± 1. The results of *DQ vs De* shown in Figure 3 indicate visible differences between the data obtained with the coarse and the refined meshes, but qualitatively the supercritical bifurcation characteristic of this flow transition to an asymmetric flow is satisfactorily captured. Nevertheless, we note that the discrepancy in *De* for a given *DQ* between the coarse mesh and the refined mesh used in [14] is only of the order of 5%, thus justifying the use of the mesh illustrated in Figure 2 for the three-dimensional simulations in this preliminary parametric study. The critical *De* is here 0.317, while it is 0.309 in Poole et al. [14], a relative difference of less than 3 %.

Results and Discussion

In Figure 4 we compare the streamline patterns on the center plane ($z = 0$) and near the walls ($z/H = \pm 1/2$) of the cross slot for the Newtonian (subcritical) and *De* = 0.4 (supercritical) cases. The

two-dimensional limiting flow and the $AR = 1$ flow cases are considered as representative examples. Although in both cases the onset of an instability that leads to asymmetric flow is observed, the flow patterns in the center plane are slightly different in each case. For the $AR = 1$ case, due to the three-dimensional nature of the flow, the asymmetry is more accentuated near the stagnation point ($x = y = z = 0$), while near the walls, at $z/H = \pm 1/2$, the flow patterns appear much more symmetric, illustrating the strong three-dimensional nature of the flow in the low *AR* geometries.

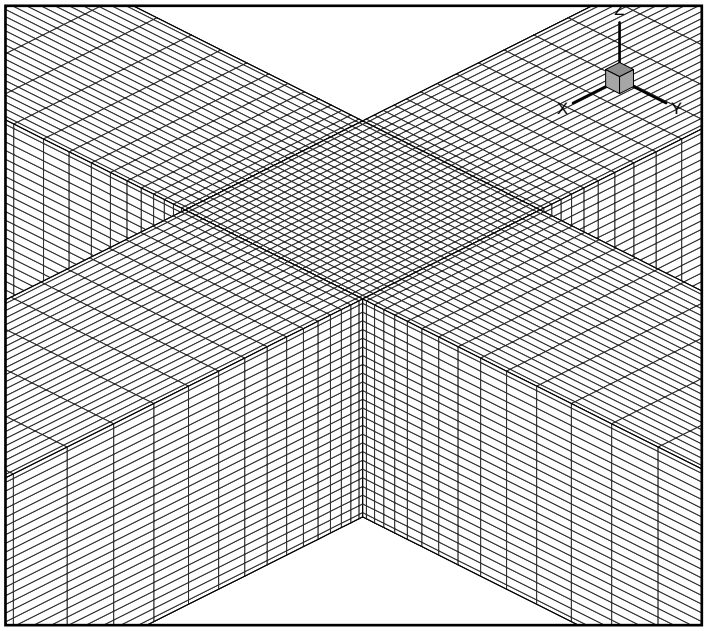

Figure 2. Computational mesh used in the simulations for the $AR = 1$ case.

For $AR \geq 1$ we found the existence of two flow transitions, the first to an asymmetric flow, followed at higher *De* values by the onset of a purely elastic periodic flow instability. For $AR \leq 0.5$ the flow patterns remained perfectly symmetric, until the onset of an elastic instability that leads to the flow becoming periodic. This time-dependent instability is triggered at progressively lower *De* values as the aspect ratio of the cross slot decreases. To summarize the numerical parametric study undertaken in this study, we find it useful to construct a map of flow pattern types. The vortex map presented in Figure 5 illustrates these flow pattern types and their location on the $\mathcal{H}$ - *De* parameter space. We have chosen to plot the dimensionless number $\mathcal{H} \equiv H/(H+D) = AR/(AR+1)$, instead of the *AR* parameter, so the values of the ordinates are bound between zero ($AR \to 0$; corresponding to the Hele-Shaw flow limit) and unity ($AR \to \infty$; corresponding to the two-dimensional flow limit) [19]. This flow map shows the existence of a narrow region where asymmetric flow can emerge, and identifies the limiting *De* for onset of time-dependent flow. This map is particularly useful to identify the operating regions where cross-slot geometries, which are often used to measure planar extensional viscosity of viscoelastic fluids, can be used to create a steady and symmetric purely-extensional flow. One important advantage of this flow configuration is that near the stagnation point the residence time is sufficiently high for the polymer molecules to attain their steady-state configuration and therefore allow the limiting steady-state extensional viscosity to be estimated.

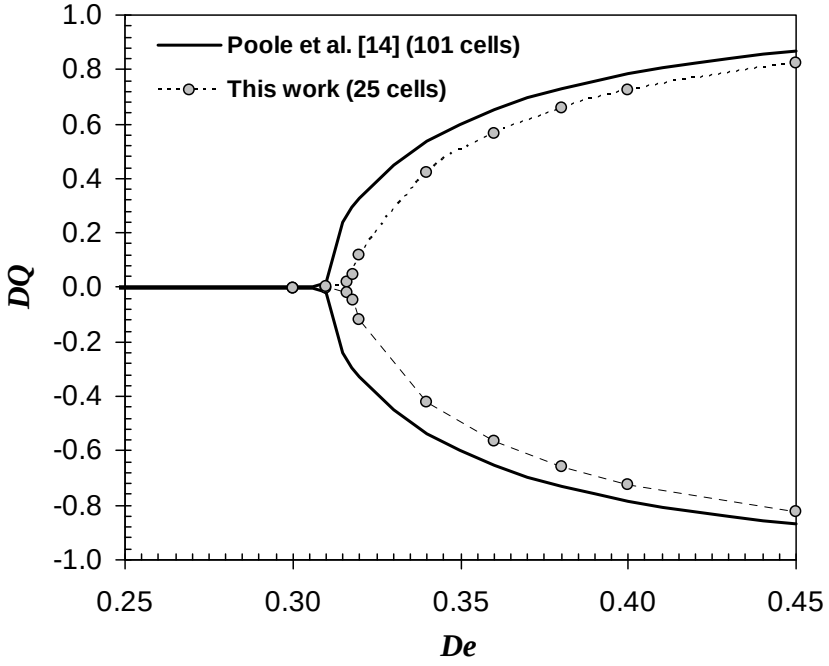

Figure 3. Predicted bifurcation plot for the limiting two-dimensional ($AR \to \infty$) case: effect of mesh refinement.

Globally, one can conclude from Figure 5 that the cross-slot walls tend to stabilize the flow, i.e. decreasing the aspect ratio there is a tendency, although not monotonic, to increase the critical *De* for the onset of asymmetric flow. Below a critical aspect ratio (around unity) the asymmetric flow does not appear and instead only the periodic instability occurs, as already discussed. This time-dependent elastic instability is found to appear at progressively smaller *De* values as the aspect ratio of the geometry decreases, i.e. as a Hele-Shaw flow is approached. This result can be explained using the criterion of McKinley et al. [4] for the onset of purely-elastic flow instabilities. According to these authors, the destabilizing mechanism which leads to such instabilities is a combination of large normal stresses (which lead to tension along the fluid streamlines) and streamline curvature. McKinley et al. [4] proposed that the curvature of the flow and the tensile stress along the streamlines could be combined to form a dimensionless criterion that must be exceeded for the onset of purely-elastic instabilities:

$$\left[\frac{\lambda U}{\Re}\frac{\tau_{11}}{\eta\dot{\gamma}}\right]^{1/2} \geq M_{\text{crit}} \tag{5}$$

where $\Re$ is the local radius of curvature, U the local streamwise velocity, τ_{11} the tensile stress and $\dot{\gamma}$ the local shear rate. The M_{crit} parameter is a constant, the exact value of which is problem dependent and is not known *a priori*. Therefore, according to this criterion, regions of flow with large tensile stresses, low streamline radius of curvature and high streamwise velocities are prone to trigger elastic instabilities. As the depth of the cross slot decreases (i.e. *AR* decreases) the shearing component (τ_{xz} and τ_{yz}) of the flow is greatly enhanced, which is beneficial in terms of stability. However, the critical

region of the flow moves towards the corners of the cross slot, where large tensile stresses develop and the streamline radius of curvature is small. Simultaneously, as the aspect ratio of the cross slot decreases, the width of the boundary layer in the *x*-*y* plane decreases (the size is of the order of *H*) and therefore *high* streamwise velocities are observed near the corner (and approaching them as *AR* decreases) in a region of high tensile stresses and low radius of curvature. The peak of maximum velocity in the center plane becomes more pronounced and moves towards the corner of the cross slot as the channel depth decreases. This effect is illustrated in Figure 6 by plotting the velocity magnitude along the line $y = -x$ in the centre plane ($z = 0$) for a Newtonian fluid and different *AR* values.

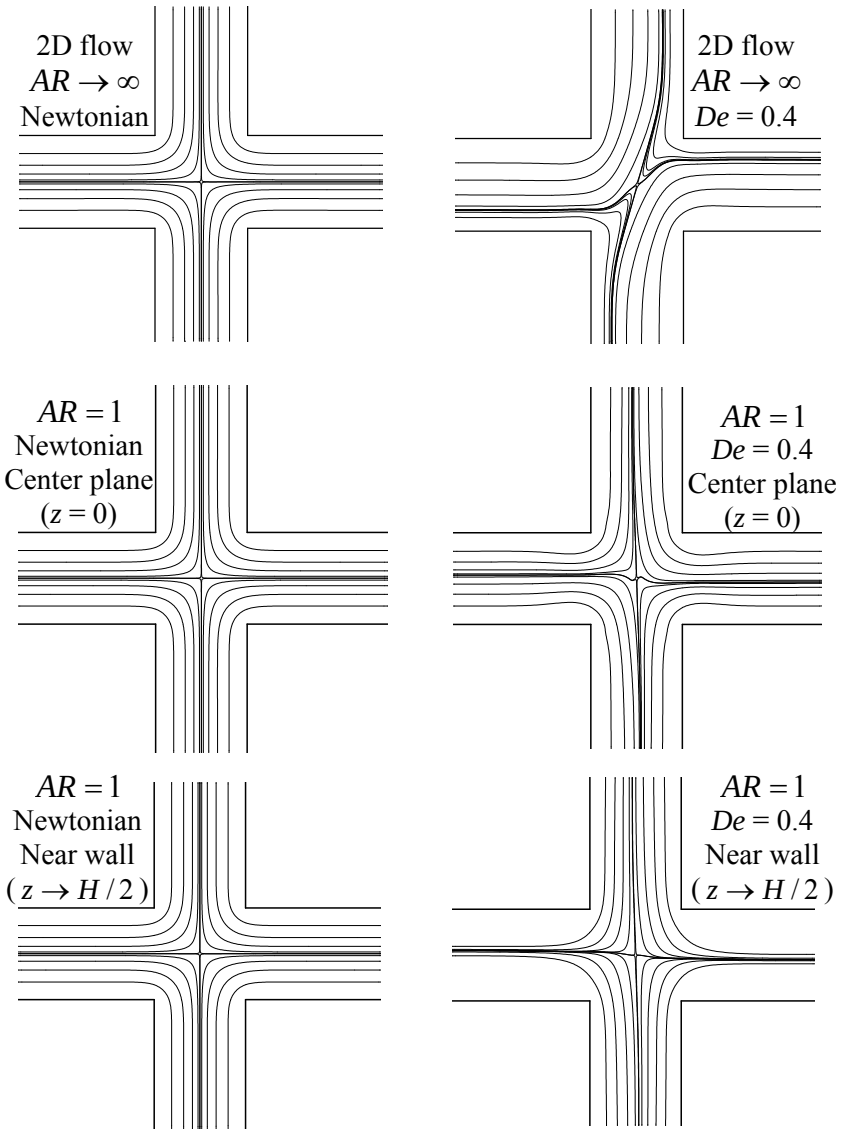

Figure 4. Comparison of predicted Newtonian and viscoelastic flow patterns for the limiting 2D case and the *AR* = 1 geometry.

For the particular case of Newtonian fluid flow this is a symmetry line of the cross-slot flow, due to the reversibility of the flow under creeping-flow conditions [20]. This shift of the maximum velocity towards the geometric singular point occurs because the perturbation imposed by the cross slot on the *x*-*y* planes does not have sufficient time to fully diffuse towards the center lines ($x, y = 0$). At the smaller depths the diffusive fluxes of momentum in the *z*-direction "dominate", compared to those in other directions, and geometry changes in *x*-*y* planes act slowly (i.e. $\Delta t_x, \Delta t_y >> \Delta t_z$ with $\Delta t_\ell \approx \ell^2 / \nu$ and $\ell = x, y, z$, with $x, y > z$). We note that for low *AR* the flow at constant *z*-planes approaches a two-dimensional potential flow, as described by Oliveira et al. [21].

Conclusions

A numerical study of the inertia-less flow of an UCM fluid in a cross-slot geometry was undertaken. The influence of the Deborah number and aspect ratio of the geometry were analyzed and a map of flow pattern types was produced. In addition, demarcation zones for the different flow regimes, i.e. symmetric steady, asymmetric steady and unsteady flow, were proposed. Knowledge of such zones may prove useful in the design of micro-fluidic chips or rheometers for example.

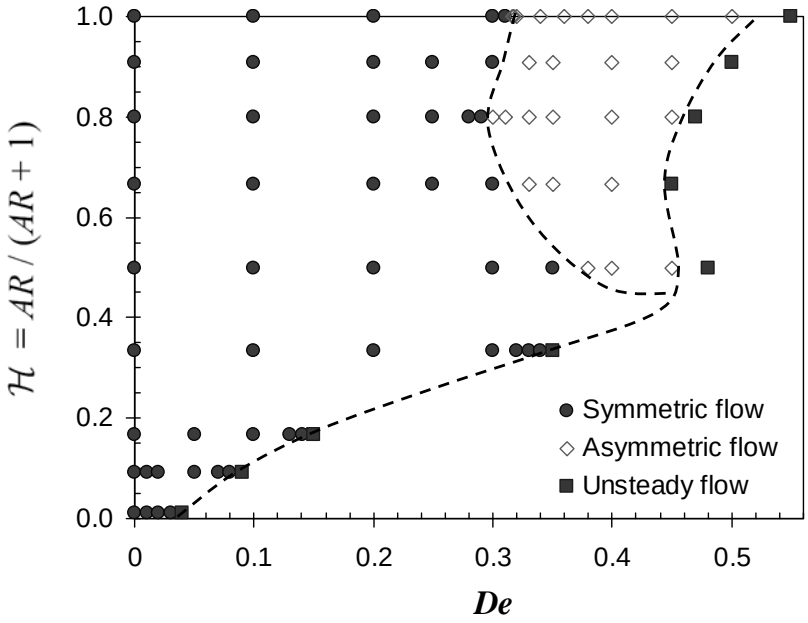

Figure 5. Flow pattern map.

Acknowledgements

The authors acknowledge the financial support from FEDER and FCT through projects POCI/EME/59338/2004, POCI/EQU/56342/2004, POCI/EQU/59256/2004, PTDC/EQU-FTT/71800/2006 and scholarship SFRH/BD/28828/2006 (A.P. Afonso).

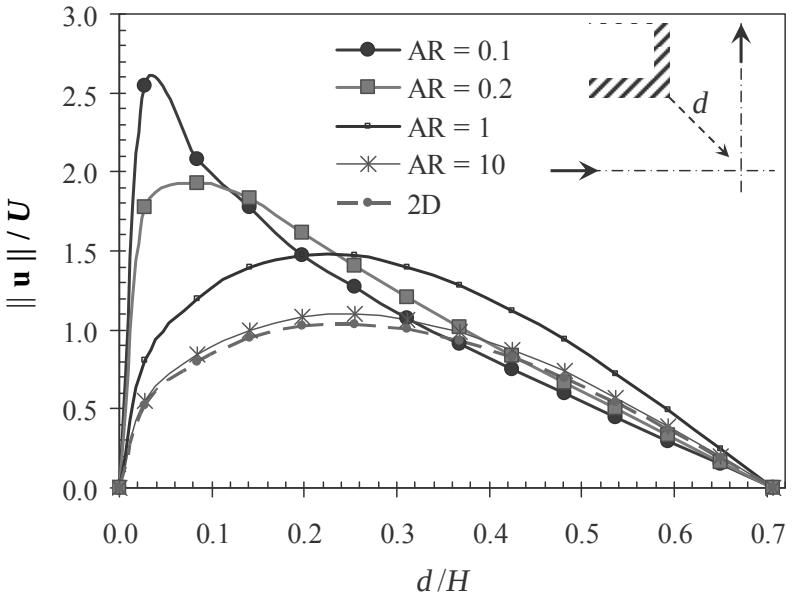

Figure 6. Influence of the geometry aspect ratio on the magnitude of velocity on the center plane ($z = 0$) for Newtonian flow along the line $y = -x$. The distance *d* is measured from the corner.

References

1. Arratia, P.E., C.C. Thomas, J. Diorio, and J. P. Gollub (2006), "Elastic instabilities of polymer solutions in cross-channel flow", *Physical Review Letters*, vol. 96, id. 144502.
2. Boger, D. V. and K. Walters (1993), "Rheological phenomena in focus", Elsevier, New York.
3. Larson, R.G., E.S.G. Shaqfeh and S.J. Muller (1990), "A Purely Elastic Instability in Taylor-Couette Flow", *J. Fluid Mech.*, vol. 218, pp. 573-600.
4. McKinley, G.H., P. Pakdel and A. Oztekin (1996), "Rheological and geometric scaling of purely elastic flow instabilities", *J. Non-Newtonian Fluid Mech*., vol. 67, pp. 19-47.
5. Pakdel, P. and G.H. McKinley (1996), "Elastic instability and curved streamlines", *Physical Review Letters*, vol. 77, pp. 2459-2462.
6. Pathak, J.A., D. Ross and K.B. Milger (2004), "Elastic flow instability, curved streamlines and mixing in microfluidic flows", *Physics of Fluids*, vol. 16, pp. 4028-4034.
7. Squires, T.M. and S. Quake (2005), "Microfluidics: fluid physics at the nanoliter scale", *Review of Modern Physics*, vol. 77, pp. 977-1026.
8. Alves, M.A. and R.J. Poole (2007), "Divergent flow in contractions", *J. Non-Newtonian Fluid Mech*., vol. 144, pp. 140-148.
9. Groisman, A. and V. Steinberg (2001), "Efficient mixing of liquids at low Reynolds numbers using polymer additives", *Nature*, vol. 410, pp. 905-908.
10. Gan, H.Y., Y.C. Lam and N.-T. Nguyen (2006), "Polymer-based device for efficient mixing of viscoelastic fluids", *Applied Physics Letters*, vol. 88, id. 224103.
11. Ottino, J.M. and S. Wiggins (2004), "Introduction: Mixing in microfluidics", *Phil. Trans. R. Soc. London A*, vol. 362, pp. 923-935.
12. Rodd, L.E., T.P. Scott, D.V. Boger, J.J. Cooper-White and G.H. McKinley (2005), "The inertio-elastic planar entry flow of low-viscosity elastic fluids in micro-fabricated geometries",

J. Non-Newtonian Fluid Mech., vol. 129, pp. 1-22.
13. Rodd, L.E., J.J. Cooper-White, D.V. Boger and G.H. McKinley (2007), "Role of the elasticity number in the entry flow of dilute polymer solutions in micro-fabricated contraction geometries", *J. Non-Newtonian Fluid Mech.*, vol. 143, pp. 170-191.
14. Poole, R.J., M.A. Alves and P.J. Oliveira (2007), "Purely-elastic flow asymmetries", *Physical Review Letters*, In Press.
15. Alves, M.A., P.J. Oliveira and F.T. Pinho (2003), "A convergent and universally bounded interpolation scheme for the treatment of advection", *Int. J. Numer. Meth. Fluids*, vol. 41, pp. 47-75.
16. Oliveira, P.J., F.T. Pinho and G.A. Pinto (1998), "Numerical simulation of non-linear elastic flows with a general collocated finite-volume method", *J. Non-Newtonian Fluid Mech.*, vol. 79, pp. 1-43.
17. Alves, M.A., F.T. Pinho and P.J. Oliveira (2000), "Effect of a high-resolution differencing scheme on finite-volume predictions of viscoelastic flows", *J. Non-Newtonian Fluid Mech.*, vol. 93, pp. 287-314.
18. Alves, M.A., P.J. Oliveira and F.T. Pinho (2003), "Benchmark solutions for the flow of Oldroyd-B and PTT fluids in planar contractions", *J. Non-Newtonian Fluid Mech.*, vol. 110, pp. 45-75.
19. Oliveira, M.S.N., L.E. Rodd, G.H. McKinley and M.A. Alves (2007), "Simulations of extensional flow in microrheometric devices", *Microfluidics and Nanofluidics*, Submitted.
20. Acheson D.J. (1990), "Elementary Fluid Dynamics", Clarendon Press, Oxford.
21. Oliveira, M.S.N., M.A. Alves, F.T. Pinho and G.H. McKinley (2007), "Viscous flow through microfabricated hyperbolic contractions", *Exp. Fluids*, vol. 43, pp. 437-451.